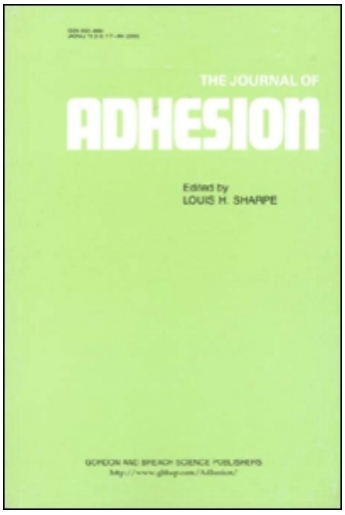

The Journal of Adhesion

Publication details, including instructions for authors and subscription information:
http://www.informaworld.com/smpp/title~content=t713453635

Two Dimensional Displacement-Stress Distributions in Adhesive Bonded Composite Structures

Juris Pirvics[a]
[a] Bell Laboratories, Murray Hill, New Jersey, U.S.A.

To cite this Article Pirvics, Juris(1974) 'Two Dimensional Displacement-Stress Distributions in Adhesive Bonded Composite Structures', The Journal of Adhesion, 6: 3, 207 — 228
To link to this Article: DOI: 10.1080/00218467408075027
URL: http://dx.doi.org/10.1080/00218467408075027

J. Adhesion, 1974, Vol. 6, pp. 207–228

Printed in Scotland

Two Dimensional Displacement-Stress Distributions in Adhesive Bonded Composite Structures

JURIS PIRVICS

Bell Laboratories, Murray Hill, New Jersey 07974, U.S.A.

(*Received July 30, 1973*)

Computerized analysis of composite structures formed by the adhesive bonding of materials is presented. The adhesive is considered to be a part of a linearly elastic system whose components are individually characterized by two bulk property elastic constants. Solution is obtained by finite difference minimization of the internal energy distribution in a discretized, piecewise homogeneous continuum. The plane-stress, plane-strain problems are considered, and yield displacement and stress distributions for the composite system. Displacement and/or stress boundary conditions are allowed. Acute contour angles are not allowed. This is the only restriction for otherwise arbitrary plane geometries.

Results are presented for typical lap shear specimens as well as for a particular case of a butt joint in which a void exists in the adhesive layer.

I. INTRODUCTION

The past thirty-five years have witnessed the expenditure of considerable analytic effort in an attempt to describe stress-strain distributions in composite structures formed by the adhesive bonding of materials. The original approximate efforts of Volkersen,[1] followed by Goland and Reissner[2] have been extended by the computerized and experimental analyses of numerous investigators. Harrison[3] and Pahoja,[4] among others, have recently added to the understanding of this rather complex problem.

To gain some insight into this composite analysis as a whole and to provide criteria for further development of bonding materials and bonding techniques, assumptions have been introduced which are justified only by the analytic tools available to the investigator. Volkerson for example, treating simple lap joints, neglects stresses originating from bending moments. Goland and Reissner incorporate part of the latter but restrict themselves to adherends of the same material having identical length and thickness, with no stress variation within the adhesive film.

With progress in analytic techniques, each succeeding investigator has been able to relax the number of assumptions previously required to obtain a solution. However, a general two-dimensional linear elasticity solution, which treats arbitrary geometries and materials with arbitrary boundary conditions, has continued to elude practical formulation and implementation.

This work is an effort intended to provide such an analytic and design tool. The plane-stress, plane-strain and axisymmetric problems are solved by finite difference minimization of the internal energy distribution in a linearly elastic body. Displacement and stress fields are generated, given displacement and/or stress boundary conditions. Composites of materials treated are each characterized by their position in a grid space and by two independent elastic bulk property constants. Acute contour angles are not allowed. This is the only restriction for otherwise arbitrary plane geometries.

Results have been obtained and are presented for typical lap shear specimens. A particular case of a butt joint in tension with a void included in the adhesive layer is also discussed.

II. STATEMENT OF PROBLEM

Consider a body, linearly elastic, piecewise isotropic, piecewise homogeneous, simply or multiply connected, infinite in one linear dimension. Material properties and geometry are invariant in that dimension. Planar cross-sections remain planar under all conditions of stress and strain and thus define a two-dimensioned problem of plane stress or plane strain. Each material block is identified by coordinates and two elastic bulk properties.

Subject the geometry under consideration to stress (normal, shear or both) displacement (one or two dimensional), or mixed boundary conditions. In the absence of body forces and thermal effects obtain displacement and stress distributions as functions of the two planar coordinates.

III. METHOD OF SOLUTION

The first law of thermodynamics for a body of volume V bounded by a surface S undergoing an adiabatic process expresses the internal energy U as

$$U = \iiint_V \text{Internal energy per unit volume} + \iiint_V \text{Increase in internal energy due to body forces acting on a unit volume element} + \iiint_S \text{Increase in internal energy due to work performed by the body on its surroundings by means of its surface displacements} \tag{1}$$

With u and w, displacements in the r (or x) and z (or y) directions respectively, Eq. (1) for an elastic body in plane strain in the absence of thermal displacements may be written in two dimensions as:

$$U(u, w) = \frac{2\pi G}{(1 - 2v)} \int\int \left\{ v\left[\frac{u}{r} + \frac{\partial u}{\partial r} + \frac{\partial w}{\partial z}\right]^2 + (1 - 2v)\left[\left(\frac{\partial u}{\partial r}\right)^2 + \left(\frac{u}{r}\right)^2 + \left(\frac{\partial w}{\partial z}\right)^2\right] + \tfrac{1}{2}(1 - 2v)\left(\frac{\partial u}{\partial z} + \frac{\partial w}{\partial r}\right)^2 \right\} r\, dr\, dz - 2\pi \int\int (F_r u + F_z w) r\, dr\, dz - 2\pi \int (\bar{F}_r u + \bar{F}_z w) r\, ds. \tag{2}$$

Where

G = Shear modulus

v = Poisson's ratio

F_r, F_z = Body forces acting on unit volume respectively in r and z directions

$\bar{F}_r, \bar{F}_z$ = Surface forces acting on boundaries

s = Contour coordinate

Solution uniqueness requires U to be a minimum, and in particular that

$$\frac{\partial U}{\partial u} = 0 \tag{3a}$$

and

$$\frac{\partial U}{\partial w} = 0. \tag{3b}$$

These last two equations, together with boundary conditions for a particular geometry form a set of two independent partial differential equations in two unknowns. The complexity of the expression for U, however, has frustrated attempts at a closed form analytic solution. Consequently, a numerical analysis approach is adopted, to be implemented on a digital computer.

The two-dimensional continuum is replaced by a grid, and differentials are replaced by difference equations at each point of a mesh formed by orthogonal grid lines, Figure 1. The physical body under consideration is represented within the confines of that mesh by straight line segments and in such a manner that all contours and changes in contour direction pass through grid points. Thus, if we consider Eq. (1) with $1/r = 0$, $r = x$ and $z = y$ we have the two-dimensional plane problem in cartesian coordinates. In

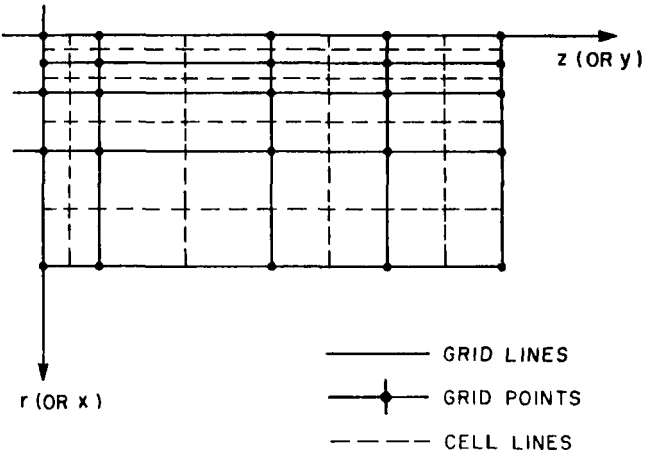

FIGURE 1 Rectangular grid.

addition, if we retain $1/r \neq 0$ we gain axisymmetric (in θ) representation with r and z as the pertinent radial and axial coordinates.

The grid mesh is further divided into cells of variable geometry to allow greater accuracy in representation, to facilitate the treatment of irregular boundaries, and to accept different material properties on adjoining sides of the grid lines. The analysis restricts itself to a finite set of twelve cells, Figure 2, a combination of which, up to a maximum of four, may be associ-

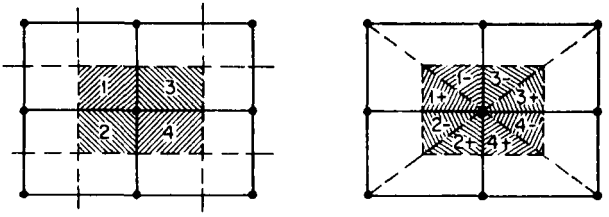

FIGURE 2 Cell types (12 allowed).

ated with any mesh point. A body can be multiply connected. Current geometries are restricted to contours which do not form acute angles because of the current selection of cell types (Figure 3).

Equations (3a) and (3b) are written for each cell and summed appropriately to represent the energy derivatives for each grid point.

Thus for an $M \times N$ grid

$$U = \sum_{i,j,k} U_{i,j,k} \qquad \begin{aligned} &i = 1, \ldots M, \quad j = 1, \ldots N, \quad k = 1, \ldots C, \\ &C = \text{number of cells associated with} \\ &\quad i,j \text{ grid point} \end{aligned} \tag{4}$$

where the internal energy for each cell is

$$U_{i,j,k} = U_{i,j,k}(u_{ij}, u_{ija}, u_{ijb}, w_{ij}, w_{ija}, w_{ijb}) \tag{5}$$

It is a function of the u and w displacements at each point considered as well as values of the displacements u and w for each of two other points (indicated by subscripts a and b) associated with each cell.

Minimization of the internal energy yields

$$\sum_{ijk} \frac{\partial U_{ijk}}{\partial u_{rs}} = 0 \tag{5a}$$

$$\sum_{ijk} \frac{\partial U_{ijk}}{\partial w_{rs}} = 0 \qquad r = 1, \ldots M, s = 1, \ldots N \tag{5b}$$

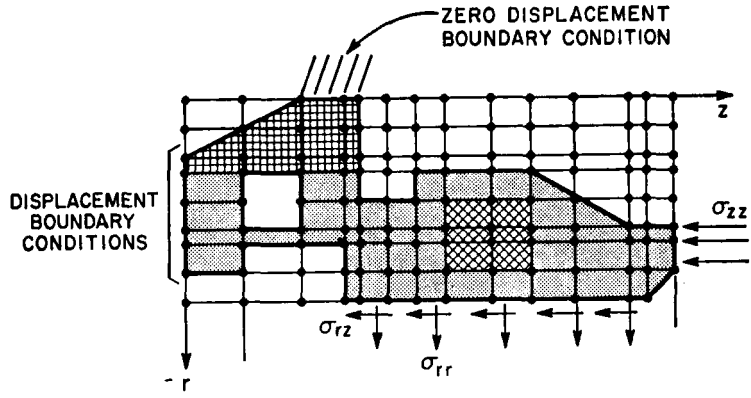

FIGURE 3 Typical application with some of possible geometries, boundary conditions and material combinations.

Thus for each point, each cell contributes information to six different equations (two for each of the three points involved by each cell).

In the absence of body forces the internal energy for each point may be written as (Appendix)

$$U_{ij} = \sum_{k=1}^{C} \sum_{l=1}^{5} D_l([Q_l]\{\varphi\})^2 + \sum_{m=1}^{2} E_m[X_m]\{\varphi\} \tag{6}$$

and its derivatives with respect to components of the placement vector become

$$\frac{\partial U_{ij}}{\partial \varphi_s} = \sum_{k=1}^{C} \sum_{l=1}^{5} 2D_l[Q_l]\{\varphi\}\frac{\partial\{\phi\}}{\partial\phi} + \sum_{m=1}^{2} E_m[X_m] = 0 \tag{7}$$

The above expression is condensed further, resulting in a general form which relates a vector of unknowns $\{\Phi_j\}$ at the jth column to those at the $j+1$ and $j-1$ columns. The relationship is established by means of

matrices consisting of elements whose values are known and a vector of constants $\{R_j\}$ in the following form

$$[A]\{\Phi_j\} + [B]\{\Phi_{j-1}\} + [C_j]\{\Phi_{j+1}\} = \{R_j\}. \tag{8}$$

Here, $\{\Phi_j\}$ is a vector of $2M$ unknowns

$$\{\Phi_j\} = \begin{Bmatrix} u_{1,j} \\ \cdot \\ \cdot \\ \cdot \\ u_{M,j} \\ w_{1,j} \\ \cdot \\ \cdot \\ \cdot \\ w_{M,j} \end{Bmatrix} \tag{9}$$

The solution is obtained by a column by column inversion technique.[5]

Given a proposed solution which relates adjacent columns of unknowns in the form

$$\{\Phi_{j-1}\} = [D_j]\{\Phi_j\} + \{E_j\} \tag{10}$$

one obtains recurrence relations which must be satisfied in the following form

$$[D_{j+1}] = [-T_j]^{-1}[C_j] \tag{11a}$$

$$[E_{j+1}] = [T]^{-1}[\{R_j\} - [B_j]\{E_j\}] \tag{11b}$$

where

$$[T]_j = [A_j] - [B_j][D_j]. \tag{11c}$$

Knowledge of boundary conditions suffices to start the recurrence relations which in turn yield the solution vectors $\{\Phi_j\}$, and thus the displacement distributions.

The stress distributions may be obtained by differentiation of the internal energy with respect to strain in the following manner.

$$\sigma_{rs} = \frac{\partial U_{ij}}{\partial \varepsilon_{rs}}, \tag{12}$$

where σ_{rs} is the [3 × 3] stress matrix and ε_{rs} is the [3 × 3] strain matrix for each point i, j.

This differentiation results in a stress–strain relationship which in turn is converted to express stresses in terms of displacements solved for in Eq. (8).

IV. APPLICATION

The preceding analysis is implemented on a digital computer using programming language FORTRAN IV on an IBM 370/165 system. A [21 × 21]

basic mesh allows 441 points for a variable two-dimensional grid representation of the geometry treated. This occupies 419,840 bytes of core on object deck execution. The routines incorporated can go to higher basic mesh sizes [25 × 25] before the matrix inversion algorithms have to be reexamined for efficiency. However, a high-density representation of this type would require extended computer memory and versions of the program in which use of intermediate scratch tapes becomes mandatory.

Typical execution time of the object deck for a single lap joint geometry with no economy accruing from use of parts of the solution existing in computer memory from the immediately preceding case is 17 seconds of CPU time.

Two particular geometries are considered to show applicability to typical geometries encountered in the adhesive bonding of materials.

The plane strain problems of a lap joint and a butt joint in tension are considered and displacement and stress distributions throughout the two dimensional x–y plane (Figures 4, 5) are investigated. The adhesive is treated as one elastic component in a three-component composite structure.

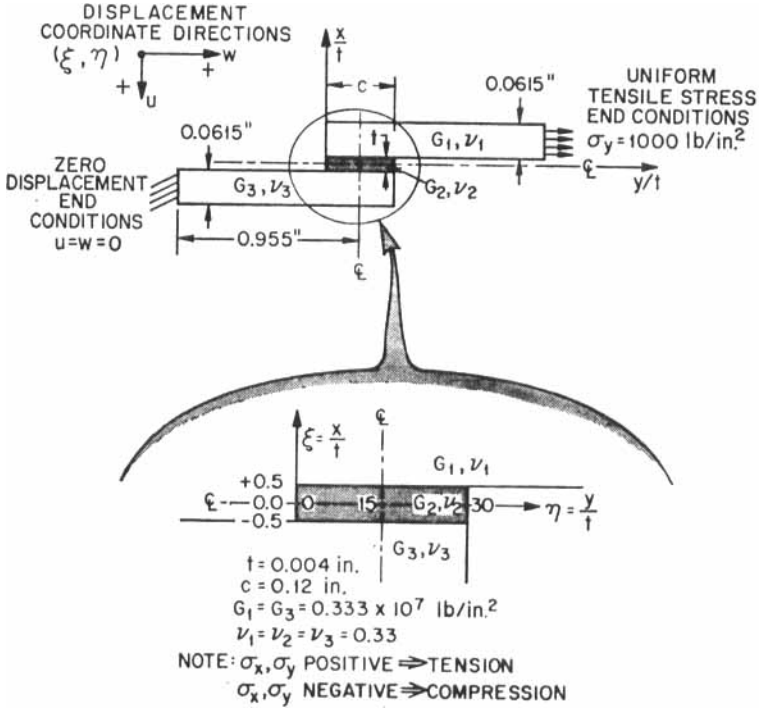

FIGURE 4 Lap joint.

The first geometry of interest is that of a lap shear joint stressed in tension at one end at 1000 psi and held at the other to zero displacement. The detailed dimensions are shown in Figure 4. The adhesive is 0.004 inch thick and exists in an aluminum overlap region which is thirty thicknesses long. The investigation also considered a complete butt joint as shown in Figure 5a. However, it was decided that to demonstrate the versatility of the analysis, a more informative treatment would deal with the simulation of a void in the

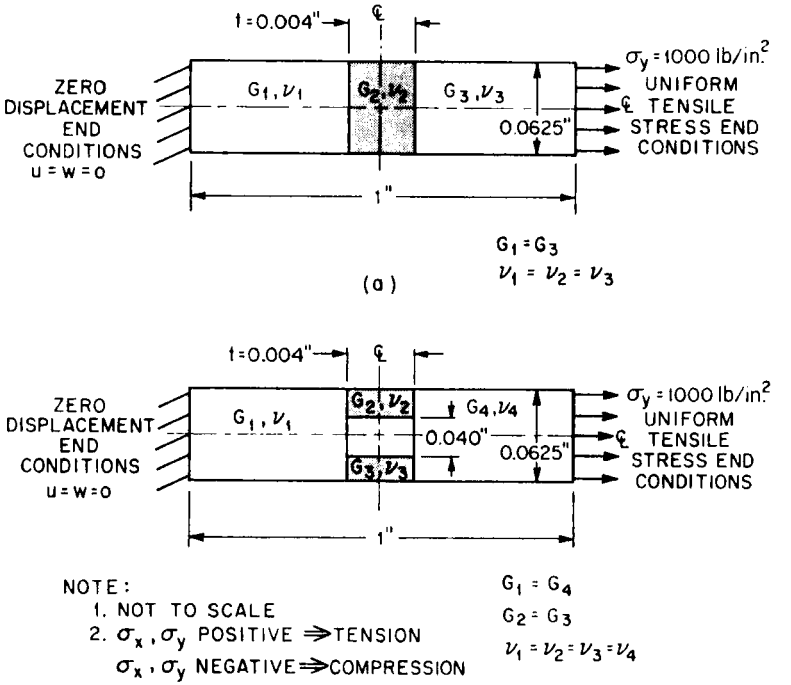

FIGURE 5 Butt joint.

adhesive material (Figure 5b). The joint is again restricted to zero displacement (u and w) at one end. At a distance of one inch a uniform tensile stress of 1000 psi is applied over the complete thickness extent (0.0625 inch). Two 0.004 × 0.0113 inch adhesive strips separated by a 0.040 inch void join the aluminum adherends.

The materials are characterized by Poisson's ratio v and shear modulus G. The former was set at 0.33 for both and G for the adhesive was allowed to assume three values, 0.4×10^5, 0.8×10^5 and 0.333×10^7. The third value is that assumed for the aluminum and thus simulates geometry effects on

a single material in response to boundary conditions. Conversely, this allows insight into the effects of material property mismatch. This mismatch in G of about two orders of magnitude is included to represent real life situations and demonstrate creation of transverse from imposed axial stress.

V. RESULTS

A. Lap joint

The region of overlap and its neighborhood evidence the largest variations in displacement and stress. Here we define axial and transverse coordinates normalized with respect to the adhesive film thickness as η and ξ respectively. Figures 6 through 13 present selected information from the total available.

Axial (w) displacements of grid lines defining the leading edge ($\eta = 0$), center ($\eta = 15$) and trailing ($\eta = 30$) cross-sections of the overlap are presented in Figure 6. The positive displacement in the direction of the applied stress is given as a function of the transverse ξ coordinate.

Three material combinations are examined. With $G_2 = 0.333 \times 10^7$ the effect of geometry is observed as we study a single material in the conventional joint configuration. We observe in particular the departure from linearity at $\eta = 0$. The sudden area change and step geometry here give rise to high stress concentrations which the material tries to depress by local deformation. The restriction to displacement imposed at the boundary where $\eta \simeq -223$ is most noted in the $\eta = 0$ transverse plane. As we proceed to the center of the overlap linearity is recovered. The geometry effect of the composite plays a decreasing role with respect to w displacement as distance increases from the leading edge of the overlap. A slight deviation is again experienced at the trailing edge. The relative w displacement for the three transverse planes is greatest at what becomes the adhesive-aluminum interface $\xi = -0.5$. This represents the material accommodation to the high normal and shear stresses generated there. The effect of the presence of a material with different properties is presented by w displacement curves for $G_2 = 0.4 \times 10^5$ and $G_2 = 0.8 \times 10^5$. First we note that the presence of the adhesive with a lower value of G_2 significantly increases the displacement of the "top" versus "bottom" aluminum layer. The adhesive deforms to drop the high stress levels generated by the geometry at $\eta = 0$. The lower the value of G_2 the greater is the displacement in the adhesive. The displacement within the aluminum "top" layer itself is essentially the same although the transverse planes move greater absolute distances due to the larger displacement of the $\xi = +0.5$ interface. Another effect of increased adhesive stress accommodation with decreased G_2 is evident in the "bottom" aluminum layer in the $\eta = 0$ plane. Here aluminum displacement increases with increased G_2.

This is not the case when $\eta = 15$ or $\eta = 30$. Farther away from the overlap leading edge at $\xi = -0.5$ displacements increase with decreased adhesive shear modulus. The necessity for this seeming paradox becomes apparent when we look at the lower interface, and consider that rotation, i.e., bending,

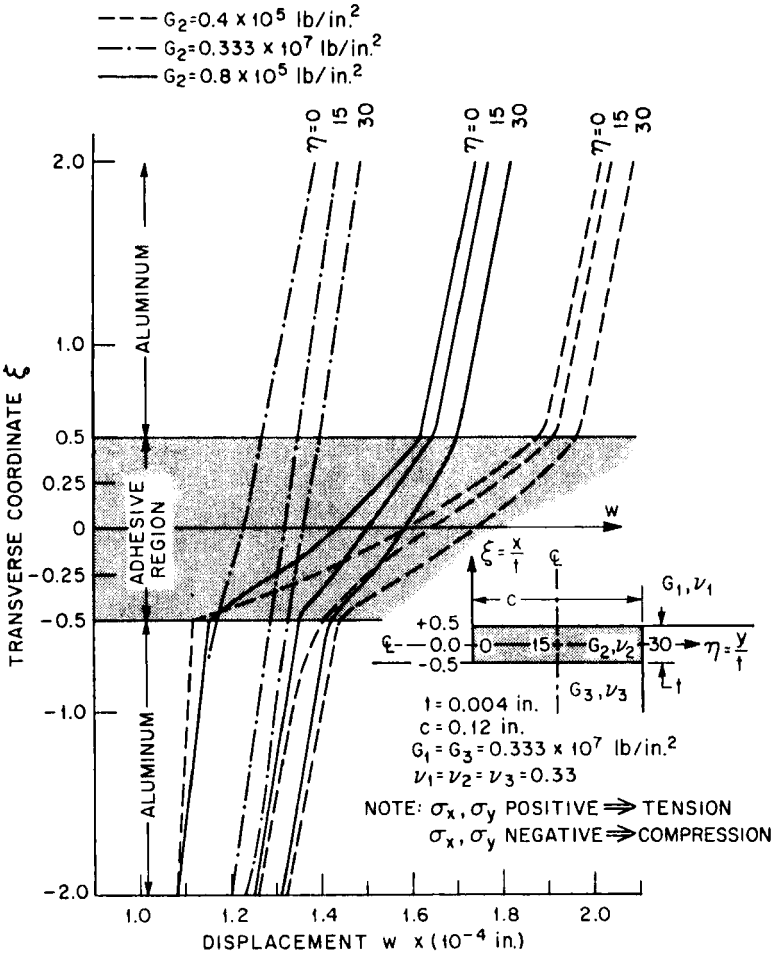

FIGURE 6 Lap joint displacement profiles in overlap region.

is taking place, Figure 7. The tensile load profile at the boundary $\eta = +223$ exerted on the "top" aluminum member aligns more easily with the "bottom" and exerts progressively greater influence on the "bottom" layer. As the adhesive attempts to decrease the stress level by displacement more and more of the aluminum becomes active in carrying the load. This phenomenon is accentuated by decrease in the adhesive shear modulus.

Planes $\eta = 30$ are displaced in w farther than $\eta = 0$ and $\eta = 15$. Therefore, the adhesive is in tension in the η direction.

Figure 7 exhibits the transverse displacement u of the two interfaces $\xi = 0.5$ and $\xi = -0.5$ for three values of G_2 as a function of the axial

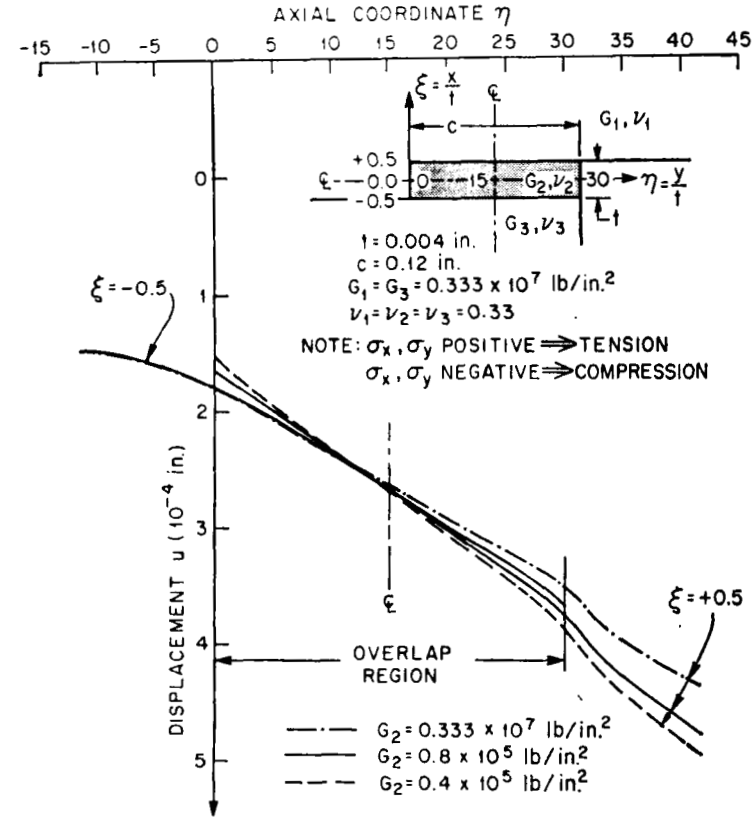

FIGURE 7 Lap joint displacement profiles in overlap region.

coordinate η. For a given material, the trailing portion of the overlap is depressed more than the leading segment. Furthermore, there exists a cross-over in the vicinity of the centerline for curves indicating upper and lower interface planes. This means that the adhesive is in tension in the leading and compression in the trailing position. This also indicates that under the existing boundary conditions transverse cleavage stress is exerted on the adhesive as the joint tries to align itself to a purely axial tensile load.

The normal stress profile for the $\eta = 0$ plane is given in Figure 8. Here the positive ξ coordinate in the curves presented is terminated at five adhesive film thicknesses because of the rapid decay to zero stress in that direction.

However, the full extent of the distribution is presented in the negative ξ direction. Here, it is interesting to note that the positive profile representing tension is reversed and indeed reveals that the lower layers of the aluminum adherend are in compression. This comes about from the bending moment exerted by the attempt on the part of the "upper" adherend to align the line of action of the tensile force boundary condition. The maximum axial stresses

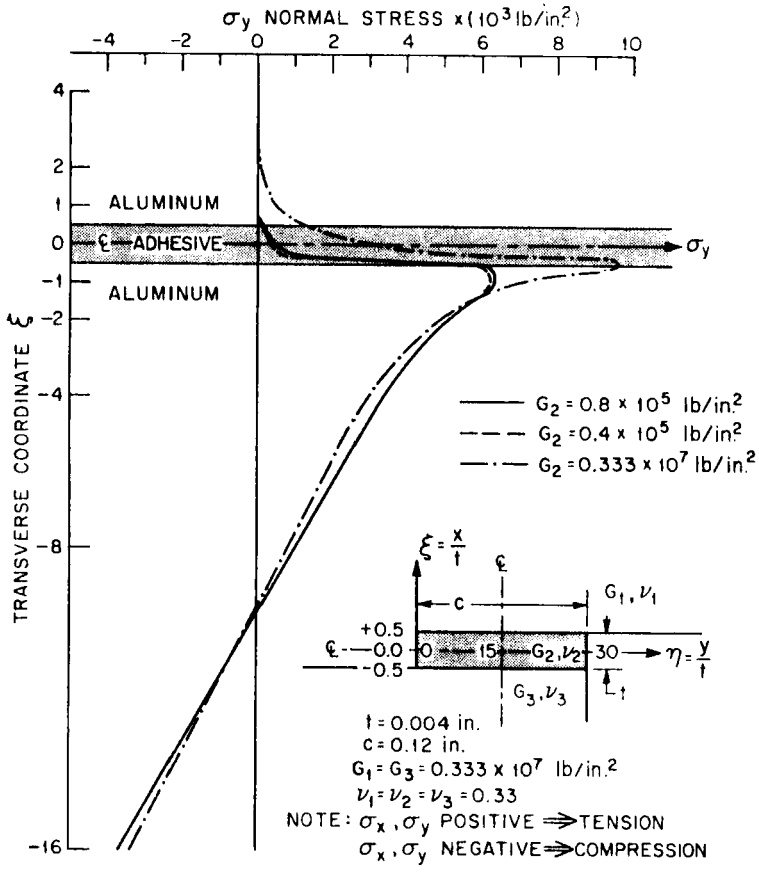

FIGURE 8 Lap joint normal stress σ_y profiles at $\eta = 0$.

are generated in materials with higher values of G_2 and occur at the $\xi = -0.5$ interface. The effect of rapid area transition is most apparent in the pure aluminum geometry. Indeed, the maximum stress level here increases by almost a complete order of magnitude relative to the average applied stress. The effects of the absence of gradual area transition and creation of stress

concentrations become apparent. The adhesive-adherend interface, even with displacement accommodation of stress concentration is faced by a stress concentration in the order of six with respect to the imposed load. The effect of lowered adhesive shear modulus with respect to that of the adherends is seen in the 30 percent reduction in maximum stress in the $\xi = -0.5$ plane. Note in particular the extent and magnitude (~ 4000 psi) of the stress reversal for all material combinations.

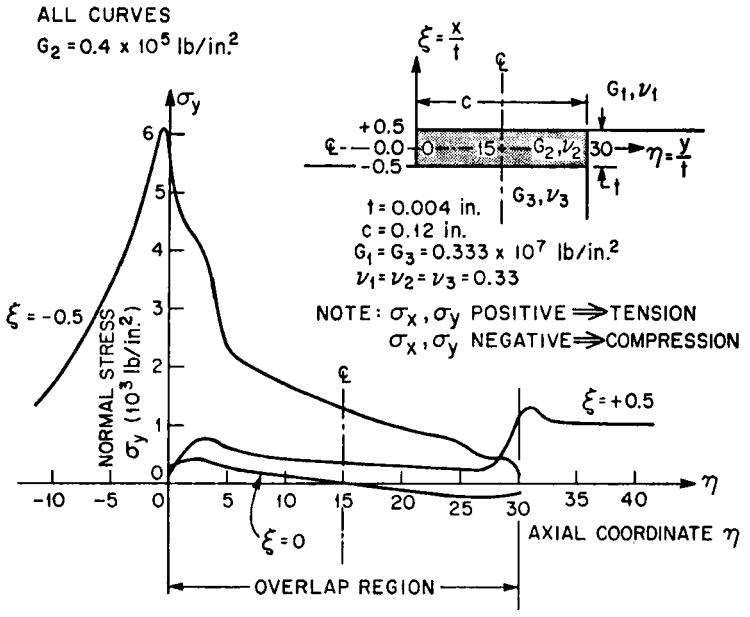

FIGURE 9 Lap joint normal stress σ_y profiles in overlap region.

Figure 9 reveals the axial variation of the σ_y stress for the three axial planes $\xi = \pm 0.5$ and $\xi = 0$ when the lowest shear modulus adhesive material is used. It is seen that the top interface is mildly loaded, reacts to the geometry within a five film thickness (0.020 inch) region at either end of the overlap and approaches the boundary condition stress within ten film thicknesses (0.040 inch) of the overlap trailing edge. The adhesive centerline reveals a leading compressive followed by a trailing tensile region previously revealed in Figure 7. The adhesive film undergoes lateral displacement and rotation and in the process undergoes changes in stress mode. The elevated stress levels are attained in the "lower" adhesive adherend interface and continue as much as 15 film thicknesses (0.060 inch) in front of the leading edge of the overlap. They extend also into the axial direction of the adhesive

but are mostly in evidence over the first 10 film thicknesses. Figure 9 thus reveals the extremely high levels of stress attained, at rapid geometric step area transitions, in both the adhesive and the adherend and directs our attention to their localized nature.

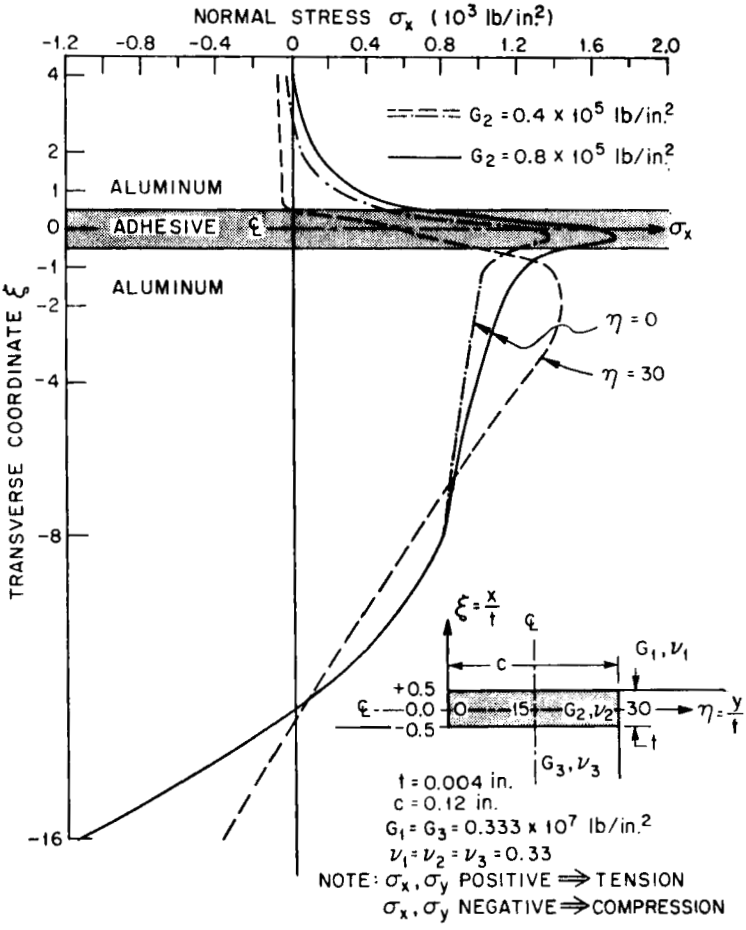

FIGURE 10 Lap joint normal stress σ_x profiles at $\eta = 0$.

The transverse normal stress σ_x created by rapid area transition and material property variation is displayed in the curves of Figure 10. The maximum stress is attained within the adhesive layer at the leading edge of the overlap. Again, the lower the shear modulus of the adhesive the lower the elevation in stress. Note that most of the adhesive carries some of the load and that the aluminum also sustains tensile as well as compressive

transverse stresses. The change in transverse distribution of the σ_x stress is compared for the same adhesive material in curves for the $\eta = 0$ and $\eta = 30$ planes. It is evident that the upper aluminum layers of the bottom adherend play an increasing load carrying capacity role for the σ_x component as we progress to the trailing edge of the overlap. Figure 11 displays the axial

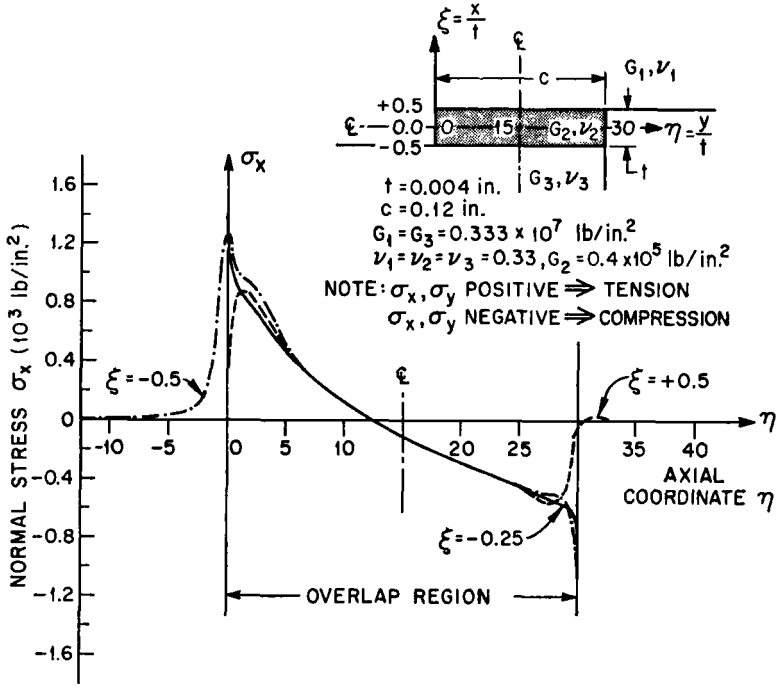

FIGURE 11 Lap joint normal stress σ_x profiles in overlap region.

variation of the transverse stress σ_x for the two interfaces and for the plane in the adhesive for which maximum stress is created ($\xi = -0.25$). It is seen that regions of high stress exist within 10 film thicknesses of the overlap in the leading edge and 5 in the trailing edge neighborhood. The reversal of stress from tensile to compressive is noted again as it occurs within a few film thicknesses prior to the centerline of the overlap.

The shear stress component distributions are explored in Figures 12 and 13. Once again, it is observed that at $\eta = 0$, maximum shear develops for the pure aluminum geometry. Stress elevation by a factor of five with respect to the average stress applied is created in the G_2, ν_2 material area. Lowering the shear modulus drops the level to that which is applied. The maximum is achieved at about a quarter of a film thickness beneath the G_2, ν_2 material

centerline and not at the interface with the G_3, ν_3 material. The presence of the lower modulus adhesive decreases the stress levels imposed on the remainder of the structure.

Figure 13 traces the axial behavior of the shear stress for aluminum and the lower-shear modulus adhesive in the two interface and highest stress

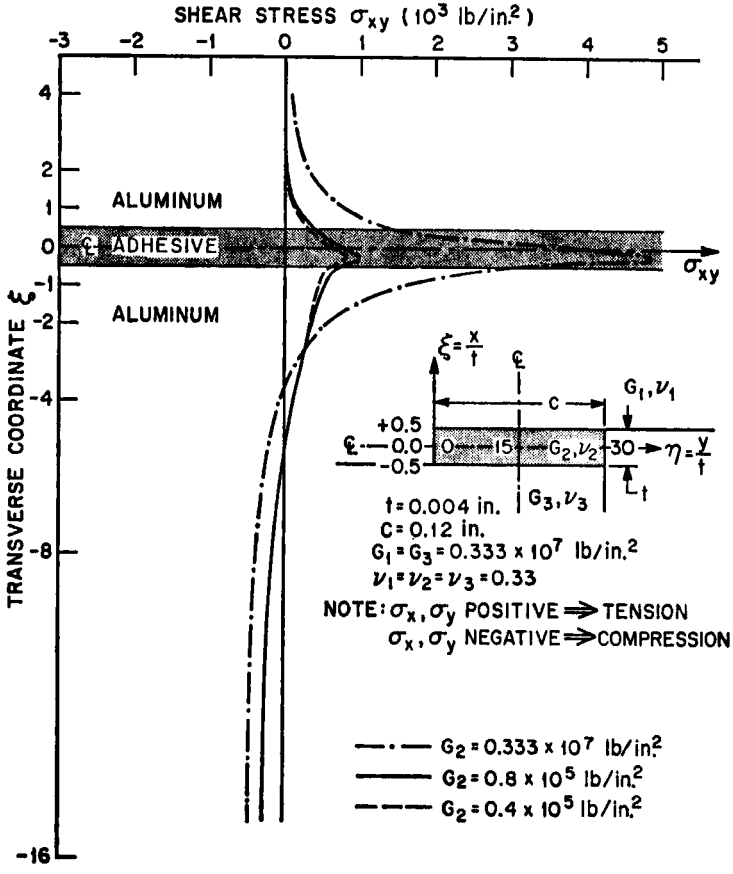

FIGURE 12 Lap joint shear stress σ_{xy} profiles at $\eta = 0$.

level planes. It is seen that the ability of the adhesive to accommodate stress levels by displacement results in strikingly lower maximum stress levels and essentially uniform shear load throughout the overlap extent. It is important to note that these interior region stress levels are higher for the adhesive than for the corresponding stiffer aluminum by about a factor of two. This behavior illustrates the capacity of the lower G material to bring more of itself into a load carrying capacity role. In both material instances maximum

shear stress is experienced within five thicknesses of the leading edge of the overlap.

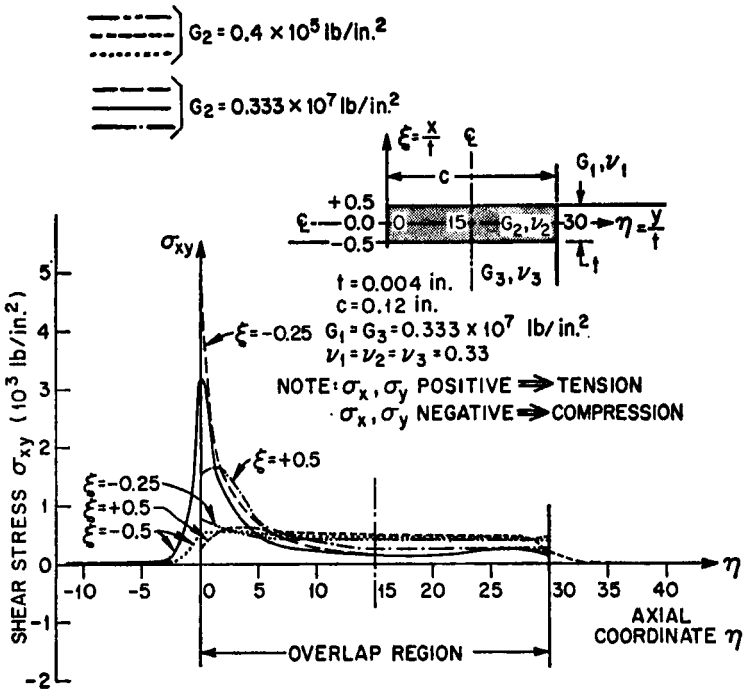

FIGURE 13 Lap joint shear stress σ_{xy} profiles in overlap region.

B. Butt joint—Void in adhesive layer

The particular geometry considered is symmetric about its axial and transverse centerlines. Most of the displacement and stress variations occur at the material and geometric discontinuities occasioned by the adhesive and by the void. We therefore focus our attention on the region which includes the adhesive and extends to the axial centerline of that void.

Figure 14 details the displacement of points in the body when it is subject to axial tension. Here the solid grid represent the unstressed state and the intersections of the dashed grid represent ends of displacement vectors from these points when the assembly is stressed. Note that referred to the solid grid scale, the scales used for displacements u and w are respectively two and one orders of magnitude larger. Thus the dashed grid displacement is exaggerated as well as biased in the representation of Figure 14.

Considering the w displacement, we see that most of it is generated by extension of the adhesive layer (in the order of 0.5×10^{-4} inch for the

0.004 inch film). The total aluminum contributes essentially the same extension in w.

The transverse deflection is negligible in the main body of the aluminum although closer to boundaries it does become noticeable. The most dramatic transverse displacement is noted in the contraction of the adhesive layer. Here the transverse adhesive motion is well over an order of magnitude

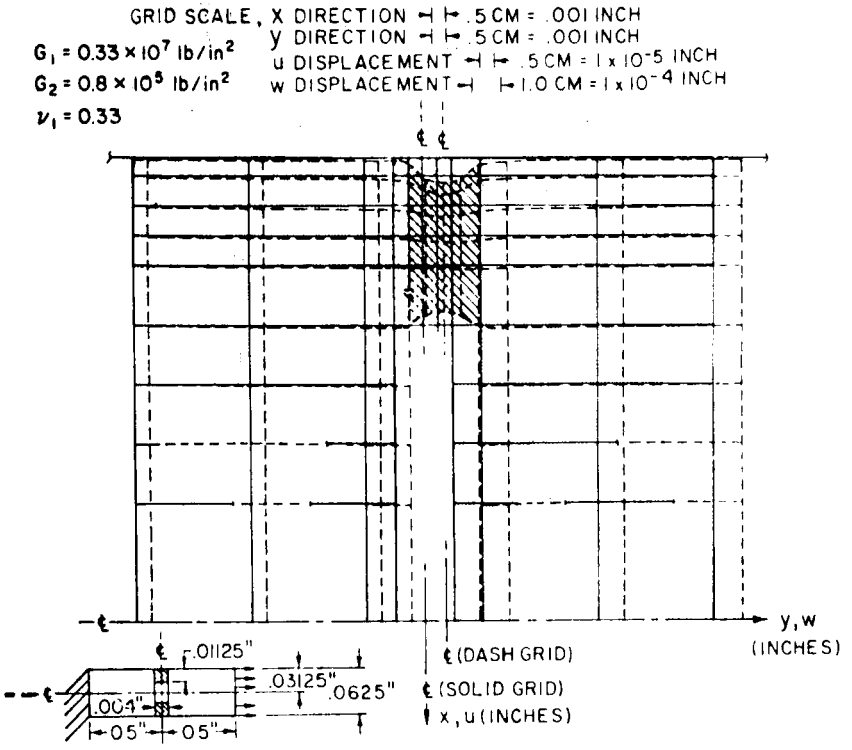

FIGURE 14 Butt joint—void in adhesive layer—detail of displacement grid.

larger with respect to that of the aluminum. Thus, the purely axial tensile boundary condition on the aluminum is translated into transverse stress as well by aluminum boundaries. The latter see the adhesive as a weak component in the assembly and act to restrict motion of the adhesive at the interfaces. The "hourglass" or characteristic "necking down" of the adhesive comes about. Note that within about five film thicknesses the transverse displacement effect of the adhesive is not discernible. This decrease in effect becomes more pronounced as we proceed toward the axial centerline. Although difficult to represent graphically, the computed results indicate

that the displaced void is not exactly rectangular, tending toward the ellipsoidal. This effect is washed out within a few film thicknesses from the void. This would account for variations in stress, and indeed transition from the tensile to the compressive mode for the σ_x stress component.

Selected curves representing the two normal stresses σ_x and σ_k are presented in Figure 15. Again, we see that within five film thicknesses (0.020 inch) of the

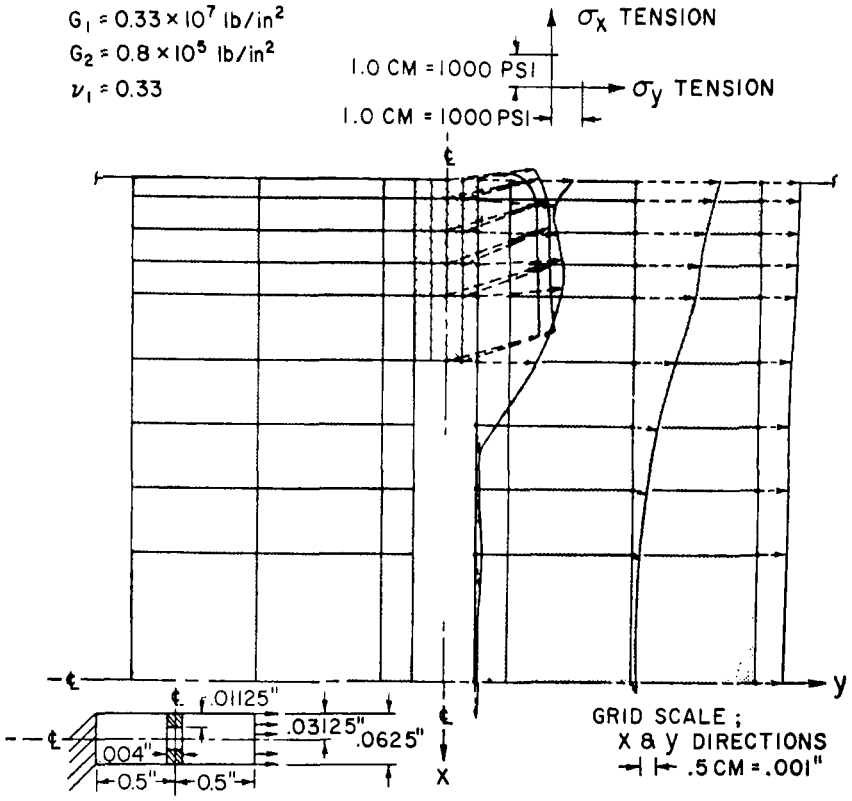

FIGURE 15 Butt joint void in adhesive layer normal stress σ_x & σ_y ($\times 10^3$).

adhesive-aluminum interface the transverse component σ_x is no longer felt and σ_y has returned to just about the uniform average σ_y load imposed 125 film thicknesses (0.5 inch) away. The stress distribution in the adhesive region has to be such that the area integrated distribution satisfies force equilibrium in the y direction. Therefore, the σ_y magnitude has to increase interior to the adhesive and immediately adjacent to it in the aluminum. As distance increases away from the interface, the axial load begins to be shared more uniformly by the aluminum.

The transverse component σ_x is always positive in the adhesive region. This is due to the Poisson's ratio effect as the adhesive attempts transverse contraction when subject to axial load as it is simultaneously restrained at the interfaces by the more rigid aluminum. The aluminum on the other hand is not so restrained and successive axial planes compress their neighbors creating the increasingly negative components in the vicinity of the void. The effect decreases in the axial direction away from the void.

VI. CONCLUSIONS

1) The computerized finite difference minimum energy approach has been demonstrated to be a viable technique in the description of adhesively bonded composite structure behavior.

2) Application to standard lap shear geometries and void-included butt joints, in addition to providing insight into these particular problems, indicates the flexibility of the analysis and predicts applicability in wider areas of interest.

3) Detailed exploration into the transverse and axial displacement-stress behavior of the assembly is a practical necessity for understanding of total composite response.

4) The demonstration of the variety of effects generated by material property differences, by boundary conditions and by geometry dictate detailed exploration for each in composite structure analysis.

Acknowledgement

Discussions of the general problem with my colleagues H. N. Vazirani and T. T. Wang in the course of this work have been most helpful. Particular appreciation is expressed for the discussions and support provided by L. H. Sharpe.

References

1. O. Volkersen, *Luftfahrtforschung* **15,** 41 (1938).
2. M. Goland and E. Reissner, *J. Appl. Mech.* **2,** A-17 (1944).
3. N. L. Harrison and W. J. Harrison, *J. Adhesion* **3,** 195 (1972).
4. M. H. Pahoja, Univ. of Illinois T. & A.M. Report No. 361, 1972.
5. V. Castelli and J. Pirvics, *Trans. A.S.M.E. J. of Lub. Tech. Series F* **89,** 177 (1967).

APPENDIX

Consider a point i, j interior to a given geometry. This point is surrounded by cells of type 1, 2, 3 and 4. The energy formulation and its derivations

must be written for each cell and then summed to represent these values for the grid point.

Formulation details are prescribed here for cell type 1, Fig. 2. With:

$$e_{ijk} = \frac{u_{ij}}{r_{ij}} + \frac{u_{ij} - u_{i-1j}}{\Delta x_{i-1}} + \frac{w_{ij} - w_{i,j-1}}{\Delta y_{j-1}} \quad \text{(dilation term)}$$

$$\omega_{ijk} = \frac{u_{ij} - u_{i,j-1}}{\Delta y_{j-1}} + \frac{w_{ij} - w_{i-1,j}}{\Delta x_{i-1}} \quad \text{(rotation term)}$$

$$a = \frac{1}{\Delta x_{i-1}}, \quad b = \frac{1}{\Delta y_{j-1}} \quad \text{(grid spacings)}$$

$k = 1$

r_{ij} = radial or x coordinate distance to ij point

G_1 = shear modulus of material associated with cell 1

ν_1 = Poisson's ratio of material associated with cell 1

Δs_{ij} = contour distance over which a force F may act.

The internal energy is written in terms of displacements u and w as:

$$U_{ijk} = \frac{2\pi G_1}{1 - 2\nu_1}\Bigg\{\nu_1(e_{ijk})^2 + (1 - 2\nu_1) \times \left[((u_{ij} - u_{i-1,j})a)^2 + \left(\frac{u_{ij}}{r_{ij}}\right)^2 + ((w_{ij} - w_{i,j-1})b)^2\right] + \frac{1 - 2\nu_1}{2}(\omega_{ijk})^2\Bigg\}\frac{r_{ij}}{4ab} - 2\pi[F_r u_{ij} + F_z w_{ij}]r_{ij}\Delta s_{ij} \tag{A1}$$

The derivatives of the internal energy with respect to each of the six displacements are:

$$\frac{\partial U_{ijk}}{\partial u_{ij}} = \frac{2\pi G_1}{(1 - 2\nu_1)}\Bigg\{\nu_1 2e_{ijk}\left(\frac{1}{r_{ij}} + a\right) + (1 - 2\nu_1)^2\left[(u_{ij} - u_{i-1,j})a + \frac{u_{ij}}{r_{ij}^2}\right] + (1 - 2\nu_1)\omega_{ijk}b\Bigg\}\frac{r_{ij}}{4ab} - 2\pi F_r r_{ij}\Delta s_{ij} \tag{A2}$$

$$\frac{\partial U_{ijk}}{\partial w_{ij}} = \frac{2\pi G_1}{(1 - 2\nu_1)}\Bigg\{\nu_1 2be_{ijk} + 2(1 - 2\nu_1)(w_{ij} - w_{i,j-1})b^2 + (1 - 2\nu_1)\omega_{ijk}b\Bigg\}\frac{r_{ij}}{4ab} - 2\pi F_z r_{ij}\Delta s_{ij} \tag{A3}$$

$$\frac{\partial U_{ijk}}{\partial u_{i-1,j}} = \frac{\pi G_1}{1 - 2\nu_1}\Bigg\{ - \nu_1 e_{ijk} - (1 - 2\nu_1)(u_{ij} - u_{i-i})a\Bigg\}\frac{r_{ij}}{b} \tag{A4}$$

$$\frac{\partial U_{ijk}}{\partial w_{i-1,j}} = -\frac{\pi G_1 \omega_{ijk} r_{ij}}{2b} \tag{A5}$$

$$\frac{\partial U_{ijk}}{\partial u_{i,j-1}} = -\frac{\pi G_1 \omega_{ijk} r_{ij}}{2a} \tag{A6}$$

$$\frac{\partial U_{ijk}}{\partial w_{i,j-1}} = \frac{\pi G_1}{(1-2\nu_1)}\left\{ -\nu_1 e_{ijk} - (1-2\nu_1)(w_{ij} - w_{i,j-1})b \right\}\frac{r_{ij}}{a} \tag{A7}$$

A more concise representation is obtained by generalizing the above formulation in terms of matrix notation. Define a 5×6 matrix Q_{lt} and a six element vector φ_t such that:

$$[Q] = \begin{bmatrix} Q_{1t} = [1/r_{ij} + a, & b, & a, & 0, & 0, & -b] \\ Q_{2t} = [b & , a, & 0, & -a, & -b, & 0] \\ Q_{3t} = [1/r_{ij} & , 0, & 0, & 0, & 0, & 0] \\ Q_{4t} = [a & , 0, & -a, & 0, & 0, & 0] \\ Q_{5t} = [0 & , b, & 0, & 0, & 0, & -b] \end{bmatrix}$$

$$\{Q\} = \begin{Bmatrix} \phi_1 = u_{ij} \\ \phi_2 = w_{ij} \\ \phi_3 = u_{i-1,j} \\ \phi_4 = w_{i-1,j} \\ \phi_5 = u_{i,j-1} \\ \phi_6 = w_{i,j-1} \end{Bmatrix} \tag{A8}$$

Then Eq. (A1) may be written as

$$U_{ijk} = D_1([Q_1]\{\varphi\})^2 + D_3([Q_3]\{\varphi\})^2 + D_4([Q_4]\{\varphi\})^2 + D^5([Q^5]\{\varphi\})^2 + D_2([Q_2]\{\varphi\})^2 + E_1[X_1]\{\varphi\} + E_2[X_2]\{\varphi\} \tag{A9}$$

and (A3–A7) with E_1, E_2, X_1, X_2, $D_t t = 1, \ldots 5$ obvious from Eq. (A1) become

$$\frac{\partial U_{ijk}}{\partial \varphi_s} = \sum_{l=1}^{5} 2D_l[Q_l]\{\varphi\}\frac{\partial\{\varphi\}}{\partial \varphi_s} + \sum_{m=1}^{2} E_m[X_m]. \tag{A10}$$